Liquid Crystal Size Selection of Large-Size Graphene Oxide for Size-Dependent N-Doping and Oxygen Reduction Catalysis

Kyung Eun Lee, Ji Eun Kim, Uday Narayan Maiti, Joonwon Lim, Jin Ok Hwang, Jongwon Shim, Jung Jae Oh, Taeyeong Yun, and Sang Ouk Kim*

Department of Materials Science and Engineering, Korea Advanced Institute of Science and Technology (KAIST), Daejeon 305-701, Korea and Center for Nanomaterials and Chemical Reactions, Institute for Basic Science (IBS), Daejeon 305-701, Korea

ABSTRACT Graphene oxide (GO) is aqueous-dispersible oxygenated graphene, which shows colloidal discotic liquid crystallinity. Many properties of GO-based materials, including electrical conductivity and mechanical properties, are limited by the small flake size of GO. Unfortunately, typical sonochemical exfoliation of GO from graphite generally leads to a broad size and shape distribution. Here, we introduce a facile size selection of large-size GO exploiting liquid crystallinity and investigate the size-dependent N-doping and oxygen reduction catalysis. In the biphasic GO dispersion where both isotropic and liquid crystalline phases are equilibrated, large-size GO flakes (>20 μm) are spontaneously concentrated within the liquid crystalline phase. N-Doping and reduction of the size-selected GO exhibit that N-dopant type is highly dependent on GO flake size. Large-size GO demonstrates quaternary dominant N-doping and the lowest onset potential (−0.08 V) for oxygen reduction catalysis, signifying that quaternary N-dopants serve as principal catalytic sites in N-doped graphene.

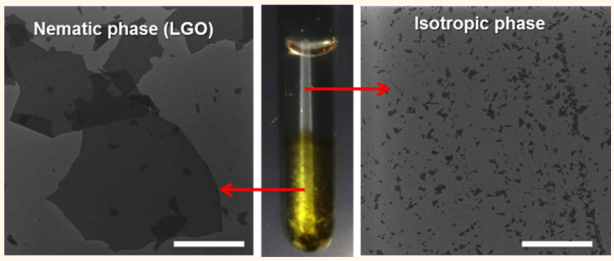

KEYWORDS: graphene · liquid crystal · doping · oxygen reduction reaction · catalyst

Graphene oxide (GO) is a typical chemically modified graphene, readily produced by the oxidative exfoliation of graphite.[1−3] The basal plane and edge of GO are decorated with oxygen functionalities, such as epoxy, hydroxyl, and carboxylic acid groups, which can facilitate spontaneous solvent dispersibility.[4] Those oxygen functional groups can also be exploited for heteroatom doping of graphene-based materials, which is highly desired for electronics,[5−7] optoelectronics,[8−10] energy storage,[11−13] and catalysis.[14,15] Meanwhile, the large shape anisotropy of two-dimensional GO may cause a discotic liquid crystalline phase in a stable dispersion.[16−19] Since our first report on the GO liquid crystal in aqueous dispersion, GO has been found to form a nematic liquid crystalline phase in various solvents, including *N*-methylpyrrollidone and dimethylformamide.[20−22]

Many physical properties of GO-based materials are known to be critically dependent on GO flake size.[23] Chemical oxidation usually generates more oxygen functionalities and defects at flake edges. Sheet resistance of the reduced GO (rGO) film is commonly limited by the high flake-to-flake resistance at residual edge defects.[24] Mechanical properties of GO paper do not meet theoretical expectation due to weakly interacting flake-to-flake junctions.[25] Consequently, large graphene oxide (LGO; flake diameter >20 μm) with a small edge to basal plane area ratio has been considered desirable for high-performance graphene-based materials. Nevertheless, poorly defined natural graphite domain size and random chemical oxidation procedure generally lead to the broad shape and size distribution of GO.[26] A few methods have been suggested for size separation of LGO, such as pH-assisted selective sedimentation[27] or density gradient ultracentrifugation.[28] Those methods facilitate delicate size selections of GO, but further purification steps are required to remove the processing additives for size selection.

* Address correspondence to sangouk.kim@kaist.ac.kr.

Received for review May 5, 2014 and accepted August 21, 2014.

Published online August 21, 2014
10.1021/nn5024544

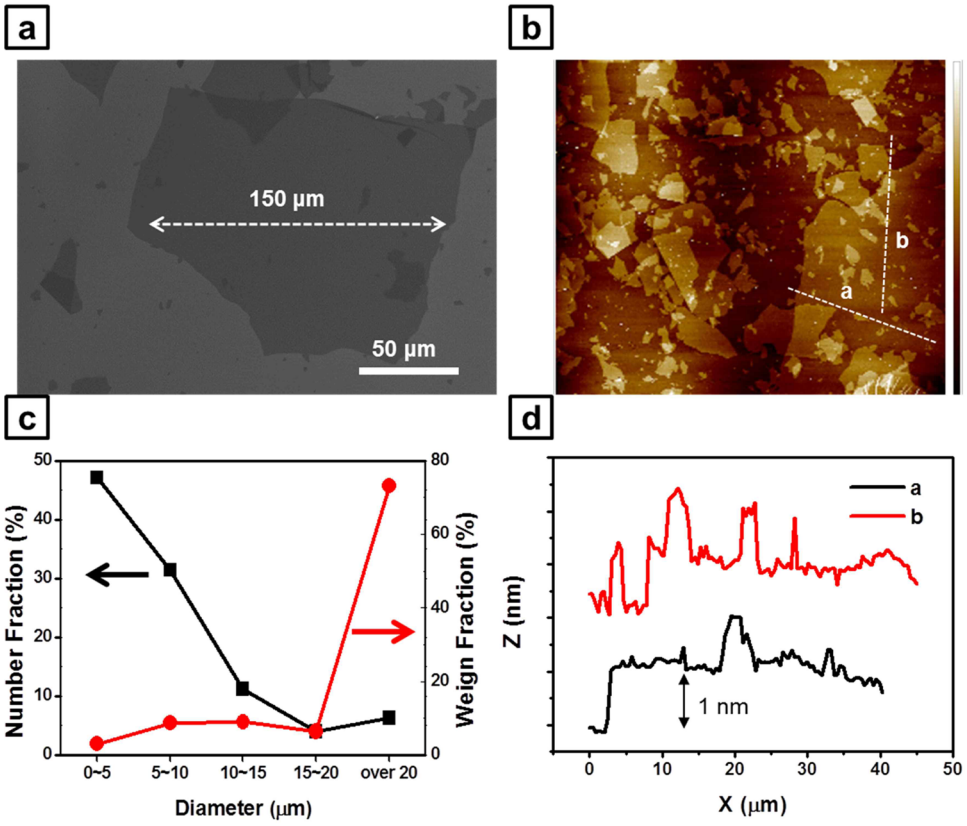

Figure 1. (a) SEM image of as-prepared GO. (b) AFM image of GO flakes. (c) Numerical fraction (black) and weight fraction (red) distributions of GO diameter. (d) Thickness profiles of GO flakes in each a and b section.

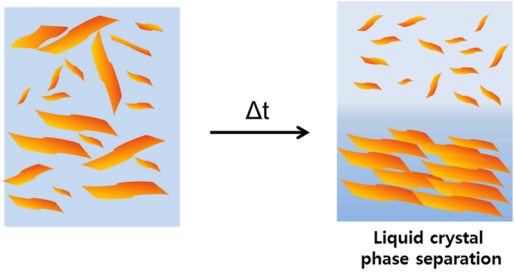

Scheme 1. Self-size separation of a GO liquid crystalline dispersion.

In this work, we introduce spontaneous, additive-free size selection of LGO flakes by liquid crystallinity and its influence on oxygen reduction reaction (ORR) catalysis behavior. Moderately concentrated GO dispersions in water spontaneously phase separate into a low-density isotropic phase and a high density nematic phase (Scheme 1). According to the well-known Onsager theory for liquid crystalline phase transition, large flakes with a high aspect ratio tend to form a nematic phase, while small flakes remain in isotropic phase.[29−33] We employed this size selection principle to investigate the influence of GO flake size on the N-doping and the resultant ORR catalysis of N-doped reduced graphene oxides (N-rGO). It is noteworthy that our work is the first report of size-dependent electrochemical properties of N-rGO. Significantly, the LGOs with small edge to basal plane ratio can accommodate quaternary-type dominant N-doping, which resulted in a high ORR catalyst performance with a small onset potential value of −0.08 V *vs* Ag/AgCl reference electrode.

RESULTS AND DISCUSSIONS

A GO aqueous dispersion was prepared by a modified Hummers method and subsequent exfoliation in water by mild shaking (Figure 1). The widely used sonication step was avoided to minimize mechanical damage and maintain the large lateral size. Instead, thorough purification by dialysis effectively removed ionic impurities such that large flakes are readily exfoliated and dispersed in water. Ionic impurities may screen the electrostatic repulsion among negatively charged GO flakes and thereby deteriorate the aqueous dispersibility.[16] Another set of small-flake GO (SGO) dispersions was prepared by addition of a sonication step as a reference (Figure S1).

In Figure 1, scanning electron microscopy (SEM) and atomic force microscopy (AFM) observations of the dried GO dispersion confirm that GO flakes have a broad distribution in their lateral size, typically ranging from 1 to 100 μm. Interestingly, although the numerical fraction of LGO > 20 μm (6.3%) is lower than smaller flakes, the weight fraction of LGOs is over 70%, due to their large molecular weight (Figure 1c). The AFM height profile measurement reveals that the GO flakes

typically have a thickness of 1 nm on a SiO_2 substrate surface, verifying monolayer exfoliation (Figure 1b,d).

Purified GO solutions were diluted to various concentrations and maintained stationary for liquid crystal phase separation (Figure 2). After 2 weeks, a sufficiently diluted GO dispersion (0.1 mg/mL) was optically isotropic, while higher concentrated solutions were macroscopically phase-separated. The liquid crystalline phase separation can be accelerated to finish within several days by the modification of container shape or mild centrifugation.[34] In this biphasic region, only the bottom phase shows bright brushes between two cross polarizers, indicating the formation of a nematic phase. The dispersion showed a complete nematic phase above the concentration of 0.8 mg/mL, which is significantly lower than the critical concentration of SGO dispersion (8 mg/mL). According to Onsager theory, the higher the aspect ratio of dispersed particles, the lower the concentration for nematic phase formation.[29−33] In this work, the broad distribution of GO flake size leads to a broad range of Flory chimneys, where both isotropic and nematic phases are equilibrated.

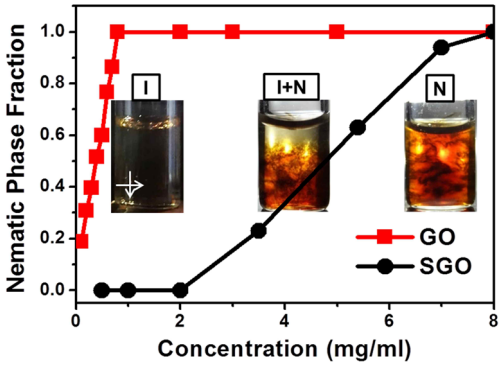

Figure 2. Nematic fraction *vs* GO concentration. (Insets) GO dispersions of 0.1, 0.6, and 1 mg/mL observed between two cross polarizers.

We investigated the composition of each phase in the completely phase-separated 0.2 mg/mL GO dispersion by SEM observation. Small GO flakes are principally concentrated in a low-density isotropic phase, while LGO flakes are predominantly concentrated in the nematic phase (Figure 3). Careful fractionation of the bottom nematic phase enables effective removal of small GO flakes and spontaneous size selection of LGO. Repeated fractionation is also possible by sequential dilution. Figure 3b compares the GO flake size distribution in a high-density nematic phase and low-density isotropic phase of 0.2 mg/mL LGO solution. Notably, LGO was never observed in the isotropic phase (Figure 3b inset graph). In this work, we employed a 0.2 mg/mL biphasic dispersion as a standard composition for size selection of LGOs. This dispersion generates an approximately 30 vol % of nematic phase. Thus, the obtainable absolute amount of LGO is not large. Nonetheless, this low composition ensures effective size purification of large flakes with a minimal amount of small flakes in its nematic phase (S2). In Figure 4,

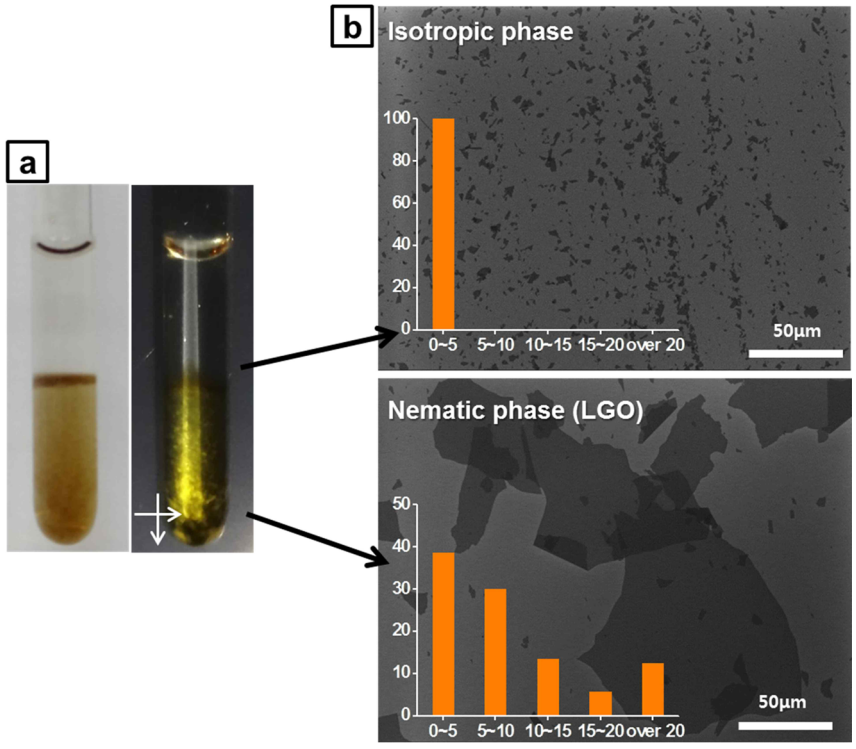

Figure 3. (a) Phase separation and (b) size selection of a GO aqueous dispersion. (Inset) Numerical fractions of GO flakes in the isotropic phase (upper) and nematic phase (below) for a 0.2 mg/mL GO dispersion.

the weight fraction of LGO flakes (>20 μm) is more than 70% prior to a size selection. After a single cycle of size selection, the weight fraction of LGO is enhanced up to even more than 90%.

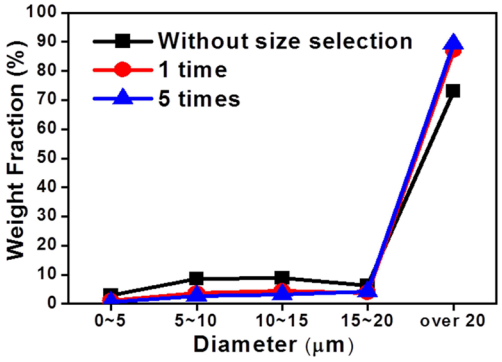

Figure 4. Statistical diameter distributions of GO after one and five liquid crystal size selections.

Substitutional doping of a heteroelement is a robust route to control and diversify the material properties of graphitic carbons.[6,35] In particular, N-dopants may effectively control the carrier density and workfunction with excess delocalized electrons and modify the surface energy and reactivity by introducing permanent dipoles. Substitutional N-dopants may exist in several different types, including quaternary (N_Q) and pyridinic (N_P). Since each dopant type may influence the material properties in a different way, selective doping of specific dopants is highly desired for many relevant applications.[36,37]

We systematically investigated the influence of flake size on the N-doping of graphene-based materials. Freeze-dried LGO and SGO aerogels were reduced and N-doped by a two-step process, as we previously reported.[8] First, the aerogels were chemically reduced by hydrazine vapor. Hydrazine is a well-known nitrogen doping source that leaves pyrazoline-like

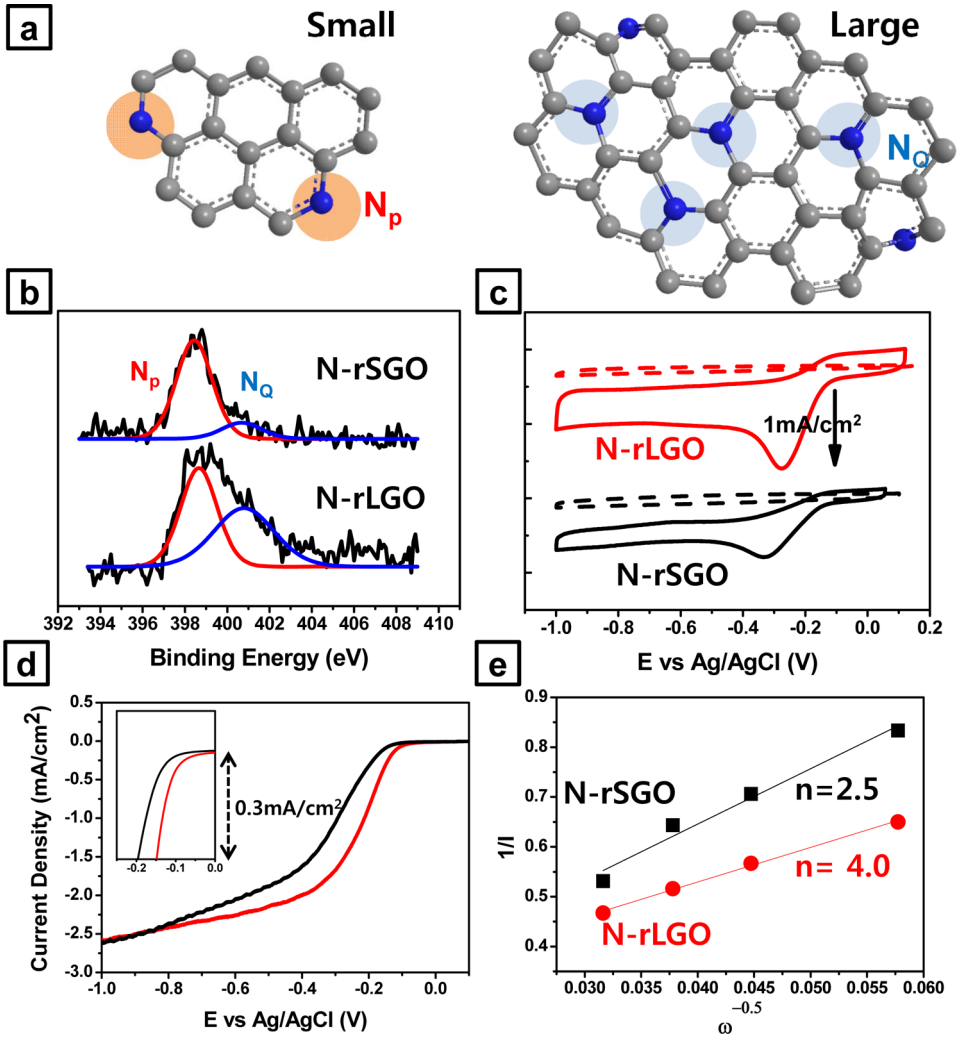

Figure 5. (a) Schematic illustration of pyridinic N dominant SGO (left) and quaternary dominant LGO (right). (b) N 1s XPS deconvolution results for N-rSGO and N-rLGO. (b) Cyclic voltammetry of N-rSGO and N-rLGO in N_2 (dash) and O_2 (line) saturated 0.1 M KOH aqueous dispersions. (d) Linear sweep voltammograms of N-rSGO (black) and N-rLGO (red) electrodes in an O_2-saturated 0.1 M KOH aqueous solution. Scan rate was 10 mV/s and rotational rate was 1000 rpm. (e) Koutecky–Levich plots of ORR at −0.5 V *vs* Ag/AgCl.

functional groups at the edge of flakes through chemical reaction with ketones.[38] Hydrazine treatment of the SGO (N/C = 0.082) with a higher density of edge functional groups shows two times higher nitrogen content than hydrazine-treated LGO (N/C = 0.047) (S4). Subsequent high-temperature treatment under a NH_3 environment restores the graphitic structure to form N-doped reduced GO.[39,40] Figure 5b shows the X-ray photoelectron spectroscopy (XPS) analysis for N-doped reduced LGO (N-rLGO) and N-doped reduced SGO (N-rSGO). Interestingly, XPS N 1s scan results demonstrate that different N-doping structures are observed depending on flake size. While the N_P peak is dominant in N-rSGO, it rapidly decreases in N-rLGO. While the total N atomic fraction decreases from 4.5% (SGO) to 2.7% (LGO), the N_Q fraction slightly increases from 1.09% (SGO) to 1.29% (LGO) (Table 1). This result demonstrates that N-doping type is controllable with GO flake size in the same N-doping condition, and N_Q is dominant when the flake size is large (low edge to plane area ratio). Different N-doping phenomena are also confirmed by ultraviolet photoelectron spectroscopy measurements. The workfunctions of N_Q abundant N-rLGO (−4.37 eV) are significantly lower than N_P dominant N-rSGO (−4.44 eV) (Table 1 and Figure S8).

Since the first report on the catalysis of N-doped graphene by L. Dai *et al.*,[41] it has been controversial which type of N-dopant is more active for ORR. Both N_Q and N_P have been suggested to facilitate ORR, but experimental and theoretical results have been inconsistent.[42−49] We measured ORR catalytic activity of our N-rGO electrodes prepared from different flake sizes and investigated the catalytic activities. We note that the electrodes were prepared by sufficient sonication such that the electroconductivity difference arising from N-rGO flake size is minimized and the measured ORR catalytic activities are dominantly dependent on N-doping types (see Materials and Methods section for details). First, cyclic voltammetry was performed in both N_2 (dash) and O_2 (line) saturated 0.1 M KOH electrolytes (Figure 5c) at a scan rate of 100 mV/s. While redox reaction was negligible in a N_2-saturated electrolyte, a distinct ORR potential peak was obtained at −0.4 V in O_2-saturated electrolyte. In linear sweep voltammograms, the onset potential is positively shifted in N-rLGO (−0.08 V) compared to N_P dominant N-rSGO (−0.11 V) (Figure 5d). In addition, N-rLGO showed the highest steady-state catalytic current density even though the total atomic percentage of N-dopant (2.7%) is low (see Table 1). We note that Nyquist plots obtained from electrochemical impedance spectroscopy show a lower charge transfer resistance of N-rLGO (42.5 Ω) compared with N-rSGO (49.5 Ω), which confirms the lower activation energy for catalytic reaction (S12).

Electron transfer numbers were calculated from the slope of a Koutecky−Levich plot (Figure 5e; see the Supporting Information). Remarkably, N-rLGO shows a four-electron reduction pathway at −0.5 V, while N-rSGO exhibits a 2.5 electron transfer number in the same conditions. Recently, several theoretical works have suggested that N_Q is a more active ORR catalytic site than N_P.[37,50−52] Highly electronegative nitrogen induces an electron acceptor state near the Fermi level, leading to partial plus charges (δ^+) to the neighboring carbon atoms.[53] Electron transfer from oxygen to the electron-deficient carbon atom may readily generate oxygen radical anions. By contrast, lone pair electrons at N_P interfere with the adsorption of oxygen and lower the binding energy of oxygen at the neighboring carbon atoms, which may result in a two-electron reduction pathway. Our experimental results are highly

TABLE 1. N-Doping Levels, Workfunction, and Electrochemical Properties of N-Doped Graphenes

	N-rSGO	N-rLGO
N [%]	4.5	2.7
N_Q [%]	1.09	1.28
N_Q/N_P[a]	0.33	0.81
Φ [eV]	−4.44	−4.37
E_{onset} [V]	−0.11	−0.08
n[b]	2.5	4.0

[a] Atomic ratio of N_Q and N_P. [b] Electron transfer number.

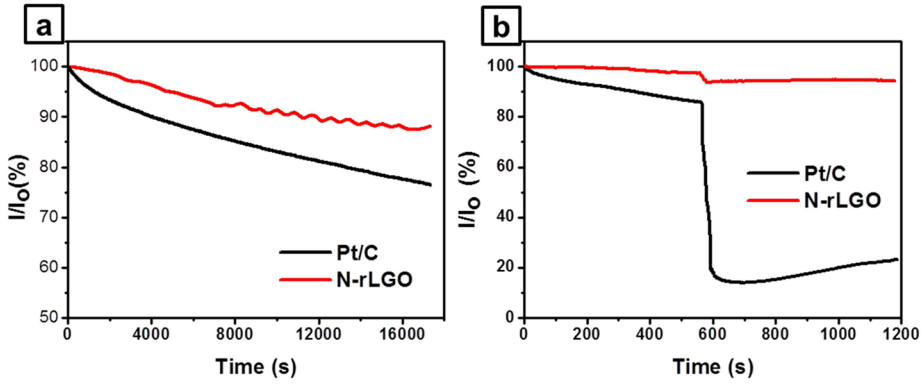

Figure 6. (a) Current−time (*I*−*t*) chronoamperometric responses of N-rsLGO and Pt/C electrodes at −0.26 V in O_2-saturated 0.1 M KOH (1000 rpm). (b) After introduction of methanol (2 wt %) at 600 s.

consistent with the theoretical predictions. N-rLGO with a lower content of N_P has a lower onset potential and a four-electron reduction pathway despite its lower total amount of nitrogen-doped sites. Overall, it is evident that N_Q dopants provide the principal catalytic sites for the ORR activity of N-doped graphene-based electrodes.

We compared the stability and possible crossover of Pt/C and N-rLGO electrodes toward ORR. In Figure 6a, we performed current−time (I−t) chronoamperometric responses to investigate the catalytic stability of Pt/C and N-rLGO in the continuous reaction at 1000 rpm in O_2-saturated 0.1 M KOH. In Figure 6b, while the current density of Pt/C decreased ∼76%, N-rLGO maintained its electrochemical activity more than 88%. This result confirms that the electrochemical activity of N-rLGO is more stable than the Pt/C electrode. Subsequently, 2 wt % of methanol, a typical fuel for fuel cells, was injected at 600 s to examine the crossover effect (Figure 4b). In the current−time chronoamperometric responses at −0.26 V in O_2-saturated 0.1 M KOH, the Pt/C electrode showed rapid decrease of current density after addition of methanol (∼75%). By contrast, N-rLGO exhibited a stable current density, demonstrating a higher selectivity toward ORR and better tolerance toward a possible crossover effect.

CONCLUSIONS

We have demonstrated the liquid crystal self-size selection principle for LGO and its effects on N-doping structures and subsequent ORR catalysis. Biphasic phase separation of LGO dispersions enables effective self-size selection of LGO. Significantly, the same N-doping condition resulted in N_Q abundant graphene film for LGO and N_P dominant graphene film for SGO, respectively. Edge-selective N-doping by hydrazine and thermal treatment facilitates such different dopant structures. Among the two principal dopant structures, N_Q effectively enhanced the ORR catalytic activity (lower onset potential) of graphitic planes even at a relatively low overall doping level. It has been well recognized that LGO leads to better electrical and mechanical properties for graphene-based materials. This work manifests that LGO also may provide a better catalytic activity with controlled dopant structures. Further advance of LGO-based catalysts is anticipated for shape-controlled, carbon-based ORR catalysis for long-term-reliable, cost-effective electrocatalysis.[54,55]

MATERIALS AND METHODS

Synthesis of Size-Selected Large Graphene Oxide. GO is prepared by a modified Hummers method. Graphite is obtained from Sigma-Aldrich (graphite, flake; batch no. 52996AJ). After filtration and washing with a 1 M HCl solution, graphite oxide was dissolved in 500 mL of water. After mild shaking, unexfoliated graphite oxides were selectively discarded through three cycles of centrifugation (5000 rpm for 30 min). After thorough dialysis (Spectra/Por dialysis membrane, MWCO: 6000−8000) for 15 days, highly pure GO solutions were obtained. For the size selection of large flakes, the GO solution was diluted to 0.2 mg/mL and placed at room temperature for 1−2 week. After complete phase separation, the top isotropic phase was gently removed by pipetting. To prepare SGO, an LGO solution was sonicated for 2 h.

Electrochemical Analysis. For the N-doping and reduction of GO, a 0.5 mg/mL GO solution was freeze-dried. The obtained GO aerogel was placed in a hydrazine vapor filled chamber for 1 h at 90 °C and thermally reduced at 750 °C under a H_2 (60 sccm) and NH_3 (40 sccm) atmosphere. Catalyst ink was prepared by mixing 1 mg of N-rGO aerogel, 800 μL of a 2-propanol−water mixture (1:3 v/v) (Sigma-Aldrich), and 21 μL of 5 wt % Nafion (Sigma-Aldrich), which was further sonicated for 30 min for stable dispersion. For the preparation of the Pt/C electrode, 5 mg of Pt/C and 16 μL of 5 wt % Nafion were mixed with 4 mL of a 2-propanol−water mixture and sonicated for 30 min. Finally, 10 μL of the ink was dropped on the glassy carbon rotating disc electrode of 5 mm diameter, which had been polished with alumina paste and cleaned by sonication. Cyclic voltammetry, linear sweep voltammograms, and chronoamperometry were performed in a three-electrode electrochemical cell, consisting of a Pt wire as a counter electrode and Ag/AgCl as a reference electrode. The electrolyte was 0.1 M KOH.

Characterization. The morphology of LGO flakes was imaged using a Hitachi S4800 SEM. Size distributions of GO flakes data were measured with Inspector 2.1 software. Raman spectroscopy was carried out with ARAMIS. N-Doping and work-functions were characterized with a VG ESCA2000 X-ray photoelectron spectrometer using a 400 μm MXR1 gun and analyzed with Avantage software. All electrochemical performance was measured by a Bio-Logic SAS SP-200 model.

Conflict of Interest: The authors declare no competing financial interest.

Supporting Information Available: Experimental methods, additional SEM, photoimages, and additional measurements. This material is available free of charge *via* the Internet at http://pubs.acs.org.

Acknowledgment. This work was financially supported by Institute for Basic Science (IBS) [IBS-R004-G1-2014-a00], and Asian Office of Aerospace Research and Development (AOARD) [AOARD-14-1403].

REFERENCES AND NOTES

1. Geim, A. K.; Novoselov, K. S. The Rise of Graphene. *Nat. Mater.* **2007**, *6*, 183–191.
2. Park, S.; Ruoff, R. S. Chemical Methods for the Production of Graphenes. *Nat. Nanotechnol.* **2009**, *4*, 217–224.
3. Li, D.; Müller, M. B.; Gilje, S.; Kaner, R. B.; Wallace, G. G. Processable Aqueous Dispersions of Graphene Nanosheets. *Nat. Nanotechnol.* **2008**, *3*, 101–105.
4. Kim, J.; Cote, L. J.; Kim, F.; Yuan, W.; Shull, K. R.; Huang, J. Graphene Oxide Sheets at Interfaces. *J. Am. Chem. Soc.* **2010**, *132*, 8180–8186.
5. Usachov, D.; Vilkov, O.; Grüneis, A.; Haberer, D.; Fedorov, A.; Adamchuk, V. K.; Preobrajenski, A. B.; Dudin, P.; Barinov, A.; Oehzelt, M.; *et al.* Nitrogen-Doped Graphene: Efficient Growth, Structure, and Electronic Properties. *Nano Lett.* **2011**, *11*, 5401–5407.
6. Maiti, U. N.; Lee, W. J.; Lee, J. M.; Oh, Y. T.; Kim, J. Y.; Kim, J. E.; Shim, J. W.; Han, T. H.; Kim, S. O. Chemically Modified/Doped Carbon Nanotubes & Graphene for Optimized Nanostructures & Nanodevices. *Adv. Mater.* **2014**, *26*, 615–619.
7. Yun, J. M.; Kim, K. N.; Kim, J. Y.; Shin, D. O.; Lee, W. J.; Lee, S. H.; Lieberman, M.; Kim, S. O. DNA Origami Nanopatterning on Chemically Modified Graphene. *Angew. Chem., Int. Ed.* **2012**, *124*, 936–939.

8. Hwang, J. O.; Park, J. S.; Choi, D. S.; Kim, J. Y.; Lee, S. H.; Lee, K. E.; Kim, Y.-H.; Song, M. H.; Yoo, S.; Kim, S. O. Work-function-Tunable, N-Doped Reduced Graphene Transparent Electrodes for High-Performance Polymer Light-Emitting Diodes. *ACS Nano* **2012**, *6*, 159–167.
9. Li, Y.; Zhao, Y.; Cheng, H.; Hu, Y.; Shi, G.; Dai, L.; Qu, L. Nitrogen-Doped Graphene Quantum Dots with Oxygen-Rich Functional Groups. *J. Am. Chem. Soc.* **2012**, *134*, 15–18.
10. Lee, J. M.; Kwon, B. H.; Park, H. I.; Kim, H. Y.; Kim, M. G.; Park, J. S.; Kim, E. S.; Yoo, S. H.; Jeon, D. Y.; Kim, S. O. Exciton Dissociation and Charge-Transport Enhancement in Organic Solar Cells with Quantum-Dot/N-Doped CNT Hybrid Nanomaterials. *Adv. Mater.* **2013**, *25*, 2011–2017.
11. Jeong, H. M.; Lee, J. W.; Shin, W. H.; Choi, Y. J.; Shin, H. J.; Kang, J. K.; Choi, J. W. Nitrogen-Doped Graphene for High-Performance Ultracapacitors and the Importance of Nitrogen-Doped Sites at Basal Planes. *Nano Lett.* **2011**, *11*, 2472–2477.
12. Lee, S. H.; Kim, H. W.; Hwang, J. O.; Lee, W. J.; Kwon, J.; Bielawski, C. W.; Ruoff, R. S.; Kim, S. O. Three-Dimensional Self-Assembly of Graphene Oxide Platelets into Mechanically Flexible Macroporous Carbon Films. *Angew. Chem., Int. Ed.* **2010**, *49*, 10084–10088.
13. Yoo, J. J.; Balakrishnan, K.; Huang, J.; Meunier, V.; Sumpter, B. G.; Srivastava, A.; Conway, M.; Reddy, A. L. M.; Yu, J.; Vajtai, R.; *et al*. Ultrathin Planar Graphene Supercapacitors. *Nano Lett.* **2011**, *11*, 1423–1427.
14. Sheng, Z.-H.; Shao, L.; Chen, J.-J.; Bao, W.-J.; Wang, F.-B.; Xia, X.-H. Catalyst-Free Synthesis of Nitrogen-Doped Graphene *via* Thermal Annealing Graphite Oxide with Melamine and Its Excellent Electrocatalysis. *ACS Nano* **2011**, *5*, 4350–4358.
15. Lee, D. H.; Lee, W. J.; Lee, W. J.; Kim, S. O.; Kim, Y.-H. Theory, Synthesis, and Oxygen Reduction Catalysis of Fe-Porphyrin-Like Carbon Nanotube. *Phys. Rev. Lett.* **2011**, *106*, 175502.
16. Kim, J. E.; Han, T. H.; Lee, S. H.; Kim, J. Y.; Ahn, C. W.; Yun, J. M.; Kim, S. O. Graphene Oxide Liquid Crystals. *Angew. Chem., Int. Ed.* **2011**, *50*, 3043–3047.
17. Behabtu, N.; Lomeda, J. R.; Green, M. J.; Higginbotham, A. L.; Sinitskii, A.; Kosynkin, D. V.; Tsentalovich, D.; Parra-Vasquez, N. G.; Schmidt, J.; Kesselman, E.; *et al*. Spontaneous High-Concentration Dispersions and Liquid Crystals of Graphene. *Nat. Nanotechnol.* **2010**, *5*, 406–11.
18. Xu, Z.; Gao, C. Aqueous Liquid Crystals of Graphene Oxide. *ACS Nano* **2011**, *5*, 2908–2915.
19. Dan, B.; Behabtu, N.; Martinez, A.; Evans, J. S.; Kosynkin, D. V.; Tour, J. M.; Pasquali, M.; Smalyukh, I. I. Liquid Crystals of Aqueous, Giant Graphene Oxide Flakes. *Soft Matter* **2011**, *7*, 11154.
20. Xu, Z.; Gao, C. Graphene Chiral Liquid Crystals and Macroscopic Assembled Fibres. *Nat. Commun.* **2011**, *2*, 571.
21. Xiang, C.; Young, C. C.; Wang, X.; Yan, Z.; Hwang, C.-C.; Cerioti, G.; Lin, J.; Kono, J.; Pasquali, M.; Tour, J. M. Large Flake Graphene Oxide Fibers with Unconventional 100% Knot Efficiency and Highly Aligned Small Flake Graphene Oxide Fibers. *Adv. Mater.* **2013**, *25*, 33.
22. Jalili, R.; Aboutalebi, S. H.; Esrafilzadeh, D.; Konstantinov, K.; Moulton, S. E.; Razal, J. M.; Wallace, G. G. Organic Solvent-Based Graphene Oxide Liquid Crystals: A Facile Route toward the Next Generation of Self-Assembled Layer-by-Layer Multifunctional 3D Architecture. *ACS Nano* **2013**, *7*, 3981–3990.
23. Su, C.-Y.; Xu, Y.; Zhang, W.; Zhao, J.; Tang, X.; Tsai, C.-H.; Li, L.-J. Electrical and Spectroscopic Characterizations of Ultra-Large Reduced Graphene Oxide Monolayers. *Chem. Mater.* **2009**, *21*, 5674–5680.
24. Zheng, Q.; Ip, W. H.; Lin, X.; Yousefi, N.; Yeung, K. K.; Li, Z.; Kim, J.-K. Consisting of Ultralarge Graphene Sheets Produced by Langmuir-Blodgett Assembly. *ACS Nano* **2011**, *5*, 6039–6051.
25. Lin, X.; Shen, X.; Zheng, Q.; Yousefi, N.; Ye, L.; Mai, Y.-W.; Kim, J.-K. Fabrication of Highly-Aligned, Conductive, and Strong Graphene Papers Using Ultralarge Graphene Oxide Sheets. *ACS Nano* **2012**, *6*, 10708–10719.
26. Pan, S.; Aksay, I. A. Factors Controlling the Size of Graphene Oxide Sheets Produced *via* the Graphite Route. *ACS Nano* **2011**, *5*, 4073–4083.
27. Wang, X.; Bai, H.; Shi, G. Size Fractionation of Graphene Oxide Sheets by pH-Assisted Selective Sedimentation. *J. Am. Chem. Soc.* **2011**, *133*, 6338–6342.
28. Sun, X.; Luo, D.; Liu, J.; Evans, D. G. Monodisperse Chemically Modified Graphene Obtained by Density Gradient Ultracentrifugal Rate Separation. *ACS Nano* **2010**, *4*, 3381–3389.
29. Onsager, L. The Effects of Shape on the Interaction of Colloidal Particles. *Ann. N.Y. Acad. Sci.* **1949**, *51*, 627–659.
30. Zhang, S.; Kinloch, I. A.; Windle, A. H. Mesogenicity Drives Fractionation in Lyotropic Aqueous Suspensions of Multiwall Carbon Nanotubes. *Nano Lett.* **2006**, *6*, 568–572.
31. Aboutalebi, S. H.; Gudarzi, M. M.; Zheng, Q. Bin; Kim, J.-K. Spontaneous Formation of Liquid Crystals in Ultralarge Graphene Oxide Dispersions. *Adv. Funct. Mater.* **2011**, *21*, 2978–2988.
32. Zhang, S.; Kumar, S. Carbon Nanotubes as Liquid Crystals. *Small* **2008**, *9*, 1270–1283.
33. Song, W. H.; Kinloch, I. A.; Windle, A. H. Nematic Liquid Crystallinity of Multiwall Carbon Nanotubes. *Science* **2003**, *302*, 1363–1363.
34. Xia, J.; Wang, J.; Lin, Z.; Qiu, F.; Yang, Y. Phase Separation Kinetics of Polymer Dispersed Liquid Crystals Confined between Two Parallel Walls. *Macromolecules* **2006**, *39*, 2247–2253.
35. Wei, D.; Liu, Y.; Wang, Y.; Zhang, H.; Huang, L.; Yu, G. Synthesis of N-Doped Graphene by Chemical Vapor Deposition and Its Electrical Properties. *Nano Lett.* **2009**, *9*, 1752–1758.
36. Yasuda, S.; Yu, L.; Kim, J.; Murakoshi, K. Selective Nitrogen Doping in Graphene for Oxygen Reduction Reactions. *Chem. Commun.* **2013**, *49*, 9627–9629.
37. Luo, Z.; Lim, S.; Tian, Z.; Shang, J.; Lai, L.; MacDonald, B.; Fu, C.; Shen, Z.; Yu, T.; Lin, J. Pyridinic N Doped Graphene: Synthesis, Electronic Structure, and Electrocatalytic Property. *J. Mater. Chem.* **2011**, *21*, 8038.
38. Park, S.; Hu, Y.; Hwang, J. O.; Lee, E.-S.; Casabianca, L. B.; Cai, W.; Potts, J. R.; Ha, H.-W.; Chen, S.; Oh, J.; *et al*. Chemical Structures of Hydrazine-Treated Graphene Oxide and Generation of Aromatic Nitrogen Doping. *Nat. Commun.* **2012**, *3*, 638.
39. Li, X.; Wang, H.; Robinson, J. T.; Sanchez, H.; Diankov, G.; Dai, H. Simultaneous Nitrogen Doping and Reduction of Graphene Oxide. *J. Am. Chem. Soc.* **2009**, *131*, 15939–15944.
40. Yang, D.; Velamakanni, A.; Bozoklu, G.; Park, S.; Stoller, M.; Piner, R. D.; Stankovich, S.; Jung, I.; Field, D. A.; Ventrice, C. A.; *et al*. Chemical Analysis of Graphene Oxide Films after Heat and Chemical Treatments by X-Ray Photoelectron and Micro-Raman Spectroscopy. *Carbon* **2009**, *47*, 145–152.
41. Qu, L.; Liu, Y.; Baek, J.-B.; Dai, L. Nitrogen-Doped Graphene as Efficient Metal-Free Electrocatalyst for Oxygen Reduction in Fuel Cells. *ACS Nano* **2010**, *4*, 1321–1326.
42. Gong, K.; Du, F.; Xia, Z.; Durstock, M.; Dai, L. Nitrogen-Doped Carbon Nanotube Arrays with High Electrocatalytic Activity for Oxygen Reduction. *Science* **2009**, *323*, 760.
43. Li, Y.; Zhou, W.; Wang, H.; Xie, L.; Liang, Y.; Wei, F.; Idrobo, J.-C.; Pennycook, S. J.; Dai, H. An Oxygen Reduction Electrocatalyst Based on Carbon Nanotube–Graphene Complexes. *Nat. Nanotechnol.* **2012**, *7*, 394–400.
44. Yu, L.; Pan, X.; Cao, X.; Hu, P.; Bao, X. Oxygen Reduction Reaction Mechanism on Nitrogen-Doped Graphene: A Density Functional Theory Study. *J. Catal.* **2011**, *282*, 183–190.
45. Yang, S.; Feng, X.; Wang, X.; Müllen, K. Graphene-Based Carbon Nitride Nanosheets as Efficient Metal-Free Electrocatalysts for Oxygen Reduction Reactions. *Angew. Chem., Int. Ed.* **2011**, *50*, 5339–5343.
46. Wohlgemuth, S.-A.; Fellinger, T.-P.; Jäker, P.; Antonietti, M. Tunable Nitrogen-Doped Carbon Aerogels as Sustainable Electrocatalysts in the Oxygen Reduction Reaction. *J. Mater. Chem. A* **2013**, *1*, 4002.

47. Geng, D.; Chen, Y.; Chen, Y.; Li, Y.; Li, R.; Sun, X.; Ye, S.; Knights, S. High Oxygen-Reduction Activity and Durability of Nitrogen-Doped Graphene. *Energy Environ. Sci.* **2011**, *4*, 760.
48. Lai, L.; Potts, J. R.; Zhan, D.; Wang, L.; Poh, C. K.; Tang, C.; Gong, H.; Shen, Z.; Lin, J.; Ruoff, R. S. Exploration of the Active Center Structure of Nitrogen-Doped Graphene-Based Catalysts for Oxygen Reduction Reaction. *Energy Environ. Sci.* **2012**, *5*, 7936.
49. Li, Q.; Zhang, S.; Dai, L.; Li, L.-S. Nitrogen-Doped Colloidal Graphene Quantum Dots and Their Size-Dependent Electrocatalytic Activity for the Oxygen Reduction Reaction. *J. Am. Chem. Soc.* **2012**, *134*, 18932–18935.
50. Bao, X.; Nie, X.; Deak, D.; Biddinger, E. J.; Luo, W.; Asthagiri, A.; Ozkan, U. S.; Hadad, C. M. A First-Principles Study of the Role of Quaternary-N Doping on the Oxygen Reduction Reaction Activity and Selectivity of Graphene Edge Sites. *Top. Catal.* **2013**, *56*, 1623–1633.
51. Kim, H.; Lee, K.; Woo, S. I.; Jung, Y. On the Mechanism of Enhanced Oxygen Reduction Reaction in Nitrogen-Doped Graphene Nanoribbons. *Phys. Chem. Chem. Phys.* **2011**, *13*, 17505–17510.
52. Liu, C. L.; Hu, C.-C.; Wu, S.-H.; Wu, T.-H. Electron Transfer Number Control of the Oxygen Reduction Reaction on Nitrogen-Doped Reduced-Graphene Oxides Using Experimental Design Strategies. *J. Electrochem. Soc.* **2013**, *160*, H547–H552.
53. Schiros, T.; Nordlund, D.; Pálová, L.; Prezzi, D.; Zhao, L.; Kim, K. S.; Wurstbauer, U.; Gutiérrez, C.; Delongchamp, D.; Jaye, C.; *et al*. Connecting Dopant Bond Type with Electronic Structure in N-Doped Graphene. *Nano Lett.* **2012**, *12*, 4025–4031.
54. Maiti, U. N.; Lim, J. W.; Lee, K. E.; Lee, W. J.; Kim, S. O. Three-Dimensional Shape Engineered, Interfacial Gelation of Reduced Graphene Oxide for High Rate, Large Capacity Supercapacitors. *Adv. Mater.* **2014**, *26*, 615–619.
55. Kim, J. Y.; Kim, S. O. Liquid Crystals: Electric Fields Line up Graphene Oxide. *Nat. Mater.* **2014**, *13*, 325–326.